RGNZ/MGPB

Seismogenic Analysis of the 2023 Mw6.9 Murghob Earthquake, Tajikistan, based on Multi-Track InSAR and Modelling

Rudarsko-geološko-naftni zbornik
(The Mining-Geology-Petroleum Engineering Bulletin)
DOI: 10.17794/rgn.2026.3.5

Original scientific paper

Rana Jaladara[1], Naufal Setiawan[1]*, Erlan Sumanjaya[2]

[1] *Geomatic Engineering, Faculty of Mineral Technology and Energy, Universitas Pembangunan Nasional "Veteran" Yogyakarta, Sleman 55283, Indonesia.*

[2] *Department of Geodesy and Geomatics Engineering, Faculty of Engineering, University of Lampung, Bandar Lampung 35141, Indonesia.*

Abstract

This study investigates the 2023 Murghob Earthquake in Tajikistan (Mw 6.9) using modelling and multi-track InSAR techniques to analyze the surface deformation and fault dynamics. The modelling approach using Pyrocko produced observation, model, and residual images, each revealing aspects of the fault geometry and rupture characteristics. Our study identified a dominant right-lateral strike-slip event, with a calculated fault strike of 128°, dip of 67°, and rake of 177°, differing slightly from previous studies. Furthermore, the modelling also suggested mixed-slip faulting, incorporating normal faulting components along the Sarez-Karakul Fault system and the Sarez-Murghab Thrust system. These findings indicate a more complex rupture process than previously emphasised in other models. Multi-track InSAR analysis supported these findings by providing high-resolution measurements of horizontal (dH) and vertical (dV) displacements. The horizontal displacements revealed significant strike-slip movements (-0.53 to 0.12 meters) along the Aksu Murghab Fault system. Meanwhile, the vertical displacements indicated substantial uplift (-0.13 and 0.32 meters), likely due to normal and thrust faulting interactions. The results highlight the complexity of the region's tectonic setting, which is influenced by multiple fault systems, including the Sarez-Karakul and Aksu Murghab faults. The study underscores the importance of integrating various geophysical methods to understand earthquake mechanisms better and improve seismic hazard assessments in tectonically active regions like Tajikistan.

Keywords:
InSAR, Multi-track InSAR, earthquake modelling, 2023 Murghob Earthquake

1. Introduction

Tajikistan is situated at the collision spot of the Indian Plate and the Eurasian Plate, moving at a speed of 20-30 mm/year (**Avouac & Tapponnier, 1993; Zhou et al., 2016**). This ongoing plate collision has formed mountainous terrain, such as the Himalayan Mountains and the Tibetan (**Tapponnier et al., 2001**). Due to frequent earthquakes stemming from this collision, Tajikistan is considered one of the seismically dangerous regions (**Singh & Ghosh, 2019**). The Pamir Mountains region, commonly called the 'Pamir Fault,' stands out as one of Tajikistan's most significant seismic zones (**Avouac & Tapponnier, 1993; Singh & Ghosh, 2019; Tapponnier et al., 2001**).

On February 23, 2023, a 6.9 in magnitude earthquake struck Murghob, Gorno-Badakhshan, Tajikistan, occurring at 00:37:38 UTC. According to information provided by the United States Geological Survey (USGS), the earthquake's epicentre was located in a seismic zone at coordinates 38.055° N, 73.229° E, at a depth of 9 km. In contrast, the Global Centroid Moment Tensor Project (GCMT) reported the recent earthquake's epicentre at 38.16° N, 73.32° E, with a depth of 14.5 km. This earthquake was notably intense, registering a value of 9 on the intensity scale and 7 on the shaking intensity scale (**USGS Earthquake Hazard Program, 2024**).

From the beginning of 2023 until March 3, 2023, the USGS recorded approximately 33 earthquakes in the area, ranging in magnitudes from 4 to 5. This region has a history of significant earthquakes, such as the one on December 7, 2015, measuring 7.2 in magnitude, and another on February 18, 1911, with a magnitude of 7.3 (USGS, 2023). The Sarez-Karakul Fault and the Aksu Murghab Fault are among the fault systems responsible for the seismic activity in the region. The Sarez-Karakul Fault currently remains active as a sinistral fault system occupying the meridian axis of the Pamir. On the other hand, the Aksu-Murghab Fault system constitutes a dextral active fault zone located southeast of the Pamir. Additionally, the Tanymas Thrust system and the Sarez-Murghab Thrust system exists (see **Figure 1**) (**Avouac & Tapponnier, 1993**).

* Corresponding author: Naufal Setiawan
e-mail address: naufal.setiawan@upnyk.ac.id
Received: 15 April 2025. Accepted: 3 November 2025.
Available online: 14 May 2026

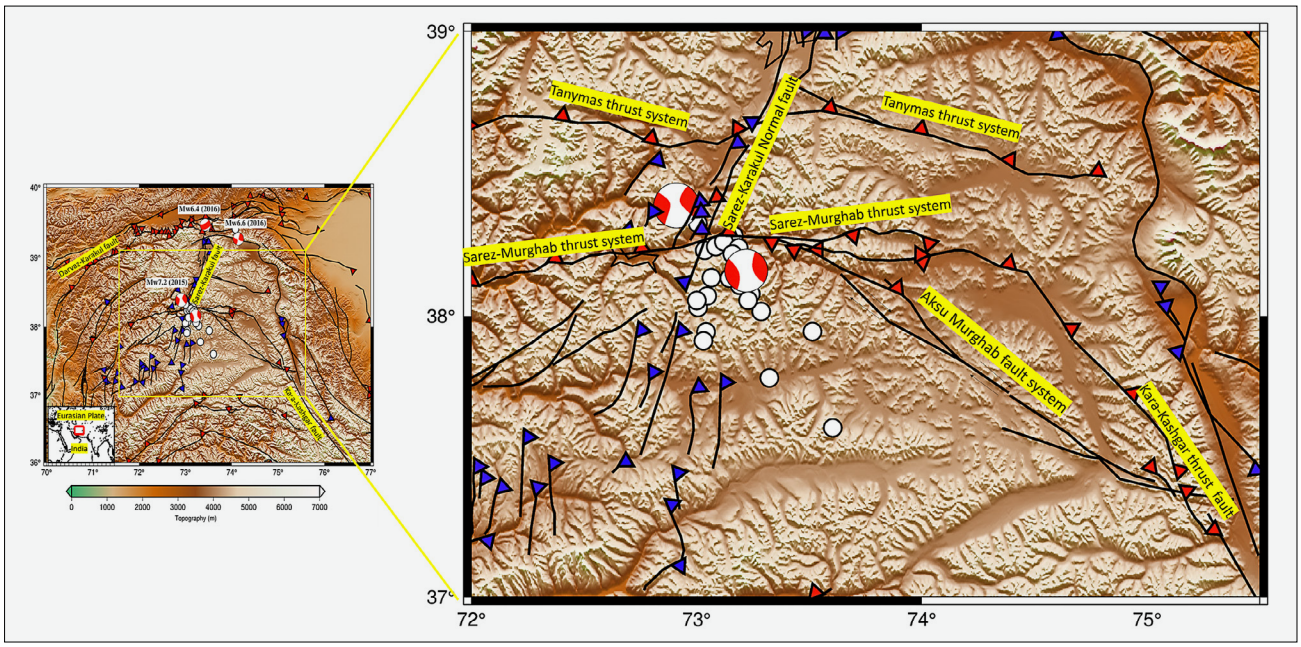

Figure 1. Tectonic setting around the 2023 Murghob earthquake. The white circles indicate aftershock events over a week. The two beach balls represent the epicentres of the 2015 Mw 7.2 and 2023 Mw 6.9 earthquakes. The lines with red triangles represent thrust faults, while the lines with blue triangles represent normal faults. The yellow box highlights the area of interest.

In geodesy, various methods are commonly employed to observe surface deformation, including the Global Navigation Satellite System (GNSS) method (**Abidin et al., 2009**) and the Interferometric Synthetic Aperture Radar (InSAR) method (**Massonnet & Feigl, 1998**). InSAR is more suitable for earthquake areas because the affected areas are often large, making GNSS less efficient (**He et al., 2023**). Moreover, GNSS observations are limited to specific receiver station locations.

Interferometric Synthetic Aperture Radar (InSAR) is a technique used to depict surface topography and surface displacement by using the phase values from two or more Synthetic Aperture Radar (SAR) images (**Furuya, 2011**). Radar waves can penetrate clouds and are effective in various weather conditions, including nighttime. The precision of InSAR can reach the centimetre level or better. InSAR works by utilizing two SAR images of the same Area of Interest (AOI) taken at different times, which are then processed to obtain range values based on phase differences. These elevation differences determine whether an area has experienced upward or downward movement.

The detection of changes on the Earth's surface using InSAR (Interferometric Synthetic Aperture Radar) has been rapidly advancing since the early 1990s. The InSAR technique calculates the interferometric phase differences between two Synthetic Aperture Radar (SAR) images, revealing changes in the terrain between the ground and the SAR instrument (**Massonnet & Feigl, 1998**). One of the pioneering studies using the InSAR method to detect changes on the Earth's surface caused by an earthquake in Landers, California. The study utilized the European Remote-Sensing Satellite-1 (ERS-1) and provided valuable insight into the potential of InSAR for earthquake monitoring and surface deformation analysis (**Massonnet et al., 1993**). Their findings significantly contributed to developing the InSAR technique as a powerful tool for studying seismic events and their impacts on the Earth's surface. Furthermore, earthquakes with a magnitude greater than 5.5 Mw and a shallow depth of less than 10 km tend to be detectable through InSAR processing techniques (**Funning & Garcia, 2019**).

Previous research on the 2023 6.9 Mw Murghob earthquake using Sentinel-1 data has yielded varied insight. The first study (**Shi, et al., 2023**) determined the total moment and identifying a 28.1° strike value based on modelling from Sentinel-1 InSAR. Furthermore, they deduced that the 7.2 Mw Sarez earthquake in 2015 initiated the 6.9 Mw Murghob earthquake. Meanwhile, (**Chen et al., 2024**) reported a dextral strike-slip fault mechanism with a maximum displacement of 0.7 meters, determined through InSAR inversion.

In this study, we investigate the 6.9 Mw Murghob earthquake using different approaches. First, we processed ascending and descending InSAR pairs utilizing Sentinel Application Platform (SNAP), followed by Forward Modelling with Pyrocko (**Heimann et al., 2017**) using the Bayesian Bootstrap Optimization (BABO) algorithm. Another notable difference is the Digital Elevation Model (DEM) used for geocoding. While the previous study (**Shi et al., 2023**) employed the Shuttle Radar Topography Mission (SRTM) DEM with a 90-meter resolution, our study implements the SRTM DEM with a

resolution of 30 meters. The accuracy of terrain correction during the InSAR processing step heavily depends on the spatial resolution of the DEM. Consequently, our results are anticipated to be more accurate, given our enhanced capability to mitigate topographic phase components. Therefore, our modelling approach supposedly has greater accuracy. Furthermore, we implement multi-track InSAR to the 6.9 Mw Murghob earthquake. Multi-Track InSAR demonstrates notable efficiency in thoroughly measuring complex displacements by decomposing surface motion into horizontal (dH) and vertical (dV) components. This methodology has been effectively utilized in examining three-dimensional displacement fields, as demonstrated in the study of the Turkey Earthquake 2023 (**Liu et al., 2024**). Previous studies have typically relied on a single InSAR pair to derive earthquake parameters, which limits the ability to resolve three-dimensional displacement fields. In this study, we address this gap by employing a multi-track InSAR methodology to enhance the analysis of surface deformation associated with the Murghob earthquake. This approach is expected to enable a more comprehensive understanding of fault dynamics by systematically decomposing line-of-sight (LOS) displacements into their horizontal and vertical components.

2. Methods

This research primarily utilizes secondary data sourced from the official website of the European Space Agency (ESA). Specifically, it employs satellite imagery from Sentinel-1A Single Look Complex (SLC) data for descending and ascending orbits. These images were accessed via the Copernicus Open Access Hub (https://scihub.copernicus.eu/dhus/#/home). Detailed information regarding the Interferometric Synthetic Aperture Radar (InSAR) data used for ascending and descending scenes in this study is provided in **Table 1**. The flowchart illustrates our research's main steps: InSAR processing, earthquake modelling, and multi-track InSAR processing (see **Figure 2**).

2.1. InSAR Processing

We utilised Sentinel Application Platform (SNAP), an open-source tool to process Sentinel-1 images, downloadable from the European Space Agency's (ESA) official website. One of SNAP's key advantages is its user-friendly graphical user interface (GUI), simplifying image processing. The processing stages include co-registration, interferogram formation, phase unwrapping, and terrain correction. Co-registration is a crucial step that aligns images by utilizing statistical values to achieve sub-pixel accuracy in spatial matching between them. This process consists of two main steps: the Apply Orbit Information step, which employs precise orbit files, and the Back Geocoding step, which uses the Shuttle Radar Topography Mission (SRTM) Digital Elevation Model (DEM) with a 1 arc-second resolution.

Table 1. Scene used for InSAR processing

Scene	Date Acquisition	Heading	Path and Frame
Ascending reference	February 3, 2023	346.6836°	Path 100, Frame 122
Ascending secondary	March 23, 2023	346.6830°	Path 100, Frame 122
Descending reference	February 21, 2023	193.2598°	Path 5, Frame 466
Descending secondary	March 5, 2023	193.2598°	Path 5, Frame 466

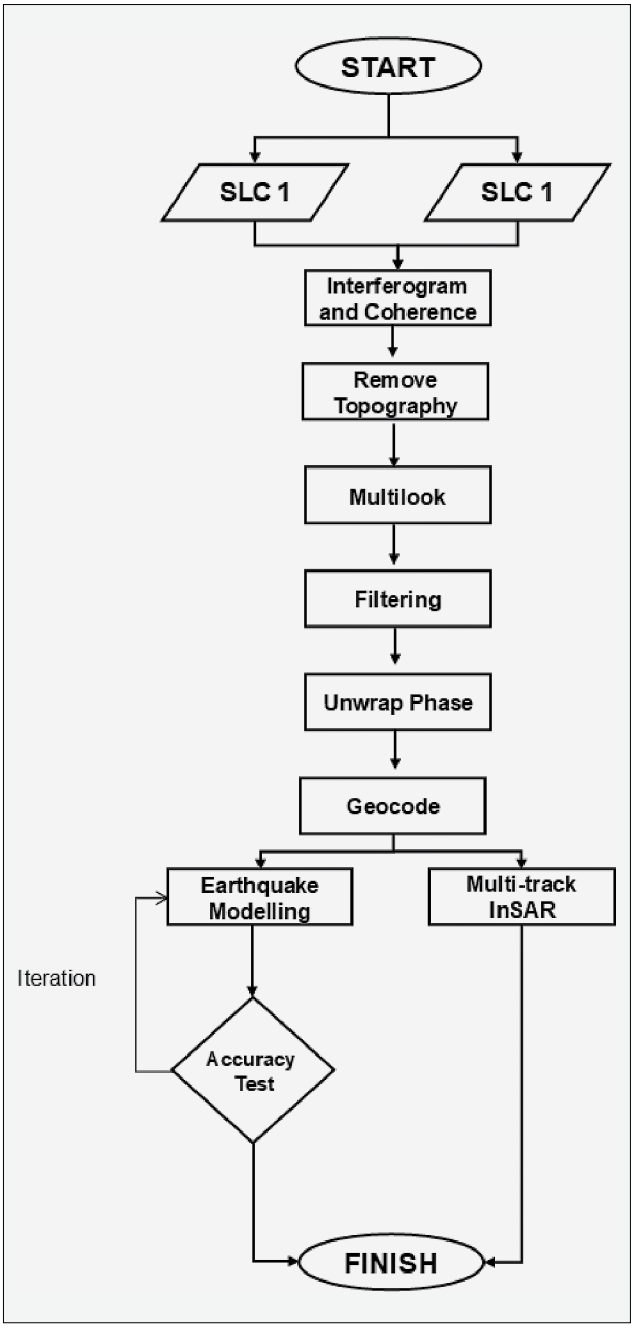

Figure 2. Research flowchart

An interferogram is generated by multiplying the reference image with the complex conjugate of the secondary image, where the amplitudes of both images are combined, and the resulting phase reflects the phase difference between the two images. The interferometric phase at each pixel of the SAR image is determined by the difference in the travel paths of the radar signals between the two SAR acquisitions to the resolution cell under consideration. The calculated interferogram exhibits phase variations (ΔØinsar) due to several contributing factors, including flat Earth phase (ΔØorb), topographic phase (ΔØtopo), atmospheric phase (ΔØatm), phase noise (ΔØnoise), and surface deformation (ΔØdefo). These components are represented mathematically, as shown in **Equation 1**.

$$\Delta\emptyset insar = \Delta\emptyset orb + \Delta\emptyset topo + \\ + \Delta\emptyset atm + \Delta\emptyset noise + \Delta\emptyset\, defo \quad (1)$$

Factors other than surface deformation (ΔØdefo) are eliminated to extract the displacement or vertical change value. The process begins with subtracting the Flat Earth Phase, which is calculated using orbit metadata and removed from the interferometric phase. Subsequently, the Topographic Phase is eliminated by differencing the interferogram data with the Digital Elevation Model (DEM). The atmospheric phase, comprising tropospheric and ionospheric components (**Furuya, et al., 2017; Setiawan & Furuya, 2021; Setiawan & Furuya, 2024**), is considered. However, for certain cases, such as large earthquakes, the phase changes due to atmospheric effects are significantly smaller than the deformation signal **(He et al., 2023**). To further reduce noise, multilooking and filtering are applied. Goldstein Phase Filtering (**Goldstein & Werner, 1998**) filters the data. Since the phase in interferometry is inherently ambiguous and confined to the range of 2π, a phase unwrapping process is necessary to connect the interferometric phase with the actual topographic height. Additionally, a multilooking process is performed after interferogram formation to optimise phase unwrapping. The multi-looking parameters used are 6 for range and 2 for azimuth. The Statistical-Cost, Network-Flow Algorithm for Phase Unwrapping (SNAPHU) (**Chen & Zebker, 2001**) is utilised for phase unwrapping. After the unwrapping process, Phase-to-Displacement Conversion and terrain correction are performed. The Phase-to-Displacement Conversion transforms the image data, measured initially in radians, into metric units (**Equation 2**). Meanwhile, the Terrain Correction process involves geocoding the image by correcting geometric distortions using the Digital Elevation Model (DEM), resulting in a georeferenced product.

$$d = -\frac{\lambda \Delta\emptyset_d}{4} \quad (2)$$

Where d is the surface displacement, λ is the wavelength, υ is Poisson's ratio, $\emptyset_d$ is the phase different.

2.2. Earthquake Modelling

Earthquake modelling in this study is conducted using Pyrocko (https://git.pyrocko.org/pyrocko), an open-source software designed for applications in seismology and geophysics. Built on the Uniplexed Information Computing System (UNIX), Pyrocko offers diverse toolboxes for analyzing and processing seismic and geophysical data. It is particularly suited for studying Earth's movements, earthquakes, and geodynamics (**Heimann et al., 2017**).

Kite, one of the toolboxes available in Pyrocko, can be used to process data from the Sentinel Application Platform (SNAP). Specifically, Kite is designed to process and analyze surface displacement data derived from InSAR (**Isken et al., 2017**). Within Kite, a data downsampling process is performed to facilitate modelling. The quadtree sampling methodology efficiently manages high-resolution Interferometric Synthetic Aperture Radar (InSAR) data. This approach subdivides the dataset into a hierarchical arrangement of tiles based on spatial variability, as illustrated in **Figure 3**. The epsilon parameter modulates the sensitivity of tile refinement, thereby ensuring that regions exhibiting significant variability are sampled at elevated resolutions, while uniform areas are represented by a smaller number of larger tiles. Parameters such as minimum tile size and maximum tile size establish the constraints for tile dimensions, thereby achieving a balance between resolution and computational efficiency. This adaptive technique facilitates effective data processing while maintaining critical spatial details, particularly in regions characterized by complex surface displacement patterns.

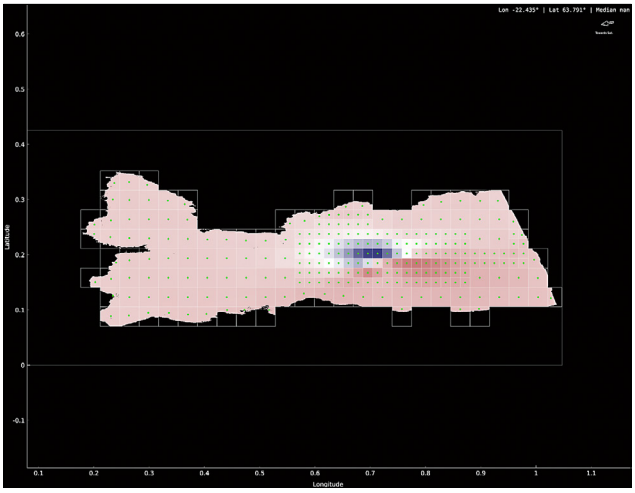

Figure 3. Downsampling of InSAR data using the Kite module. The figure illustrates how interferogram data points are reduced to representative subsets, allowing efficient modelling while preserving the main deformation signal.

Earthquake modelling in this study is performed using the Grond (**Heimann et al., 2018**) toolbox, with data imported from the Kite toolbox. To conduct modelling utilizing Pyrocko, it is essential to acquire two distinct

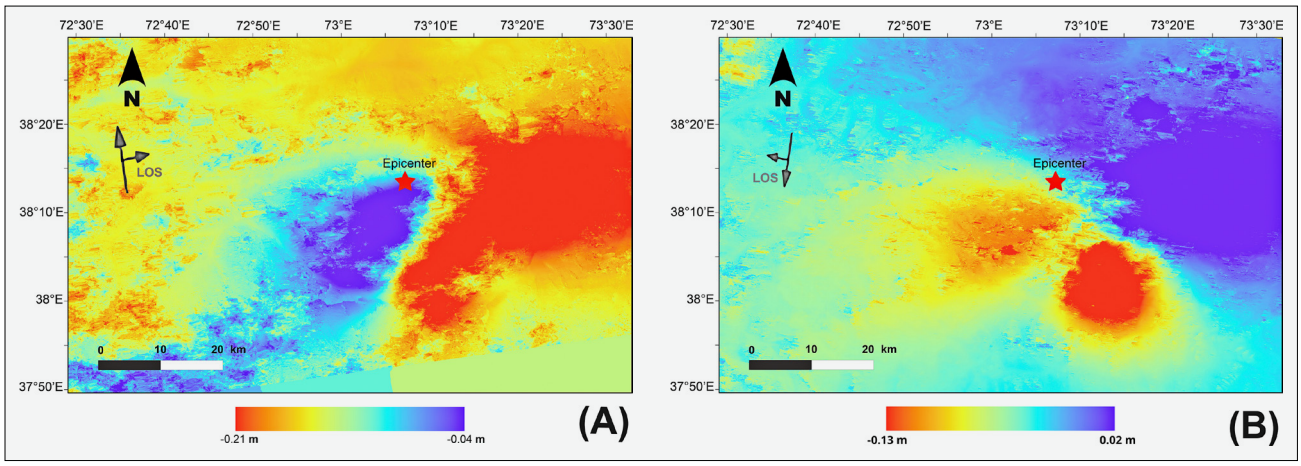

Figure 4. Unwrapped interferograms reveal coseismic deformation from the Murghob earthquake: (a) ascending and (b) descending Sentinel-1 tracks. Changes in colour gradients point to displacements in the line of sight, predominantly with maximum alterations occurring near the epicentral region. Negative measurements reveal ground displacement moving away from the satellite (subsidence), while positive measurements reflect an upward shift (uplift).

scenes, specifically those characterized by ascending and descending trajectories within the earthquake-affected region. The modelling employs a rectangular finite fault model, requiring the input of various parameters. Eight iterations are conducted, progressively increasing: 250, 500, 750, 1000, 3125, 6250, 12500, and 25000 iterations. The primary input parameters for the model include depth values, east_shift, north_shift, length, width, strike, dip, and rake. Calculations are performed using the Bayesian Bootstrap Optimization (BABO) statistical approach. BABO is a global optimization algorithm designed for multi-objective functions through directed searches. It enables the formation of a set of objective function, identifying multiple minima, irregularly shaped minima, and evaluating parameter trade-offs and uncertainties in terms of probability.

2.3. Multi-Track InSAR Processing

The multi-track InSAR approach combined multiple Sentinel-1 tracks to differentiate surface displacement's horizontal (dH) and vertical (dV) components. The dH and dV maps were derived from ascending and descending track data and thoroughly processed to ensure precise deformation characterizations. This approach facilitates enhanced discernment of horizontal and vertical movements that might remain obscured in the Line-of-Sight (LOS) data alone.

It is important to note that the multi-track technique implemented in this analysis explicitly maps the vertical (dV) and horizontal (dH) displacement dimensions. However, most SAR observation (including Sentinel-1) has a near-polar orbit, so the North-South displacement cannot be observed and produces a negligible phase change (**Equation 3**) (**Fuhrmann & Garthwaite, 2019; Fujiwara et al., 2000**). Nonetheless, complete 3D displacement from InSAR observation may be obtained if right-looking and left-looking images are available (**Wright et al., 2004**), or by combining with Global Navigation Satellite System (GNSS) observation.

$$\begin{pmatrix} v_{asc} \\ v_{des} \end{pmatrix} = \begin{pmatrix} -sin\ \theta_{asc}\, cos\ \alpha_{asc} & cos\ \theta_{asc} \\ -sin\ \theta_{des}\, cos\ \alpha_{des} & cos\ \theta_{des} \end{pmatrix} \begin{pmatrix} v_E \\ v_U \end{pmatrix} \quad (3)$$

3. Results

3.1. InSAR Result

The interferometric process using Synthetic Aperture Radar (SAR) images produces a spectral pattern known as fringes, where each concentric circle represents half the wavelength of the radar signal. These fringes were converted into unwrapped phase imagery using the SNAPHU algorithm and subsequently transformed into displacement measurements in meters. This process provides a detailed depiction of surface deformation within the research area.

Analysis of the ascending track data (see **Figure 4a**) reveals displacement values ranging from -0.21 to -0.04 meters. Similarly, the descending track data (see **Figure 4b**) indicates displacement values ranging from -0.13 to 0.02 meters. Particularly, the area surrounding the earthquake's epicenter exhibits a distinct pattern, with some regions showing significant subsidence while others experience uplift. This phenomenon is attributed to active fault movement in the region, particularly during the Murghob earthquake, highlighting the dynamic tectonic activity shaping the Earth's surface in this area.

3.2. Earthquake Modelling Result

We used the standard epsilon value of 0.04 m in the quadtree meshing method. This value was chosen to preserve minor deformation signals while preventing excessive patch subdivision from noise. A lower epsilon value would increase the number of quadtree patches,

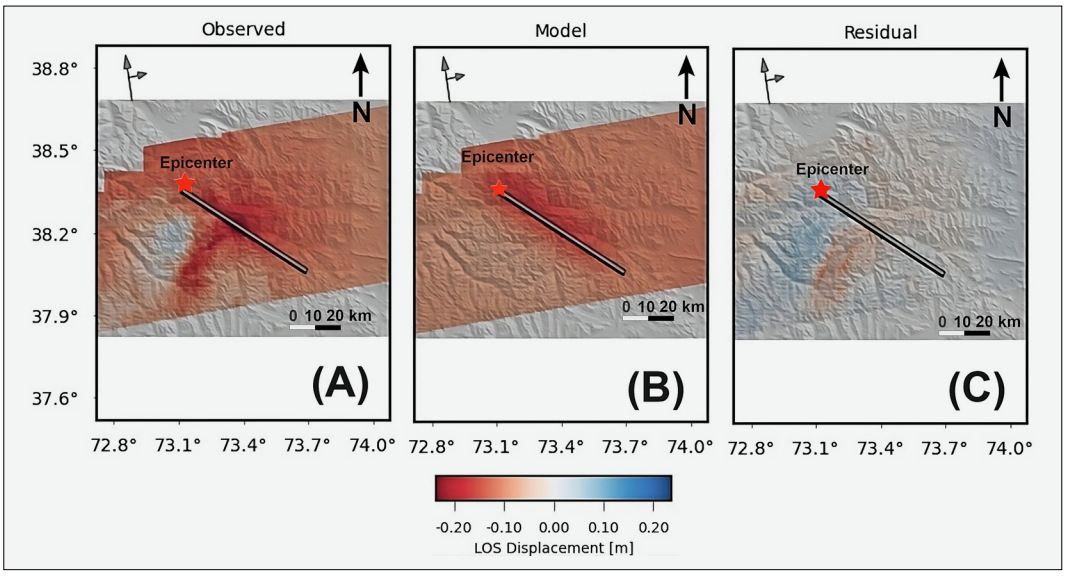

Figure 5. Modelling results for the ascending track: (A) observed displacement from InSAR, (B) best-fit synthetic model, and (C) residuals (observed–modelled). The residuals are significantly reduced, indicating the model adequately reproduces the observed deformation.

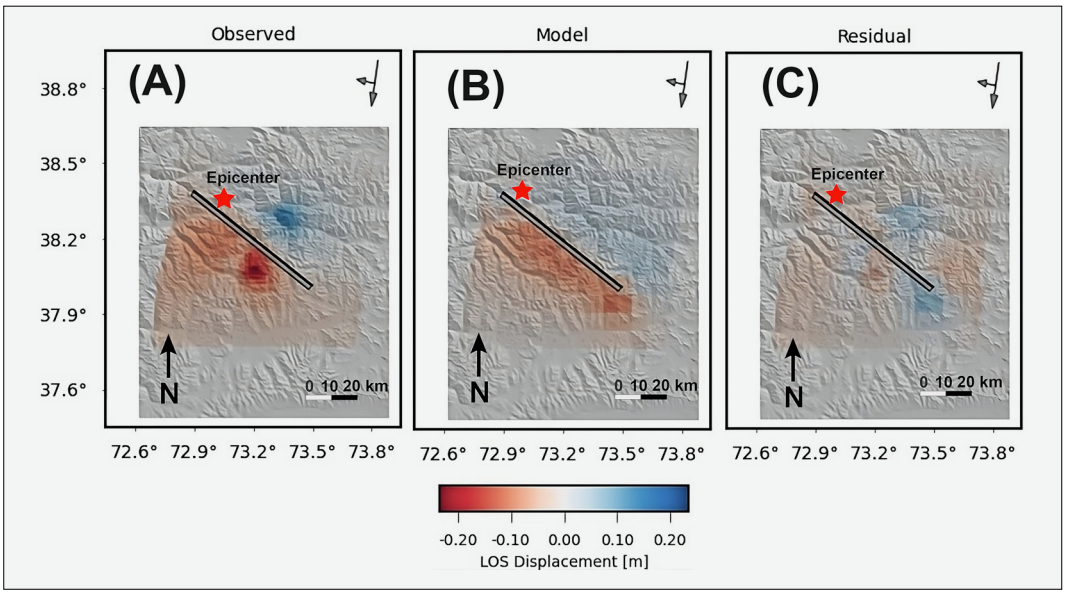

Figure 6. Modelling results for the descending track: (A) observed displacement from InSAR, (B) best fit synthetic model, and (C) residuals (observed–modelled). The residuals indicate a strong correlation between observations and model prediction, akin to the ascending track.

potentially introducing noise, whereas a higher value could smooth deformation features excessively, reducing spatial resolution.

We adjusted the prior distributions for source parameters (strike, dip, rake, depth, and slip) from their default settings for the Bayesian inversion process. These adjustments were informed by data from the USGS and GCMT assessments of the 2023 Mw 6.9 Murghob earthquake and relevant regional tectonic factors. This use of informative priors ensured that the search space accurately represented credible fault geometries for the research area. Although we did not perform a sensitivity analysis, the posterior results matched catalog solutions, suggesting that the selected priors and the standard epsilon value did not significantly bias the inversion results.

The modelling stage using Grond produces a series of images (see **Figure 5** and **Figure 6**) critical to the research analysis. These include the observed, modelled, and residual images, each serving a specific purpose in understanding the fault dynamics. The observed image represents the raw data, visualizing all available information without modifications or processing. This image serves as a baseline, capturing the unaltered characteristics of the earthquake's surface deformation. The modelled image depicts the data after being processed through the modelling software. It provides a refined

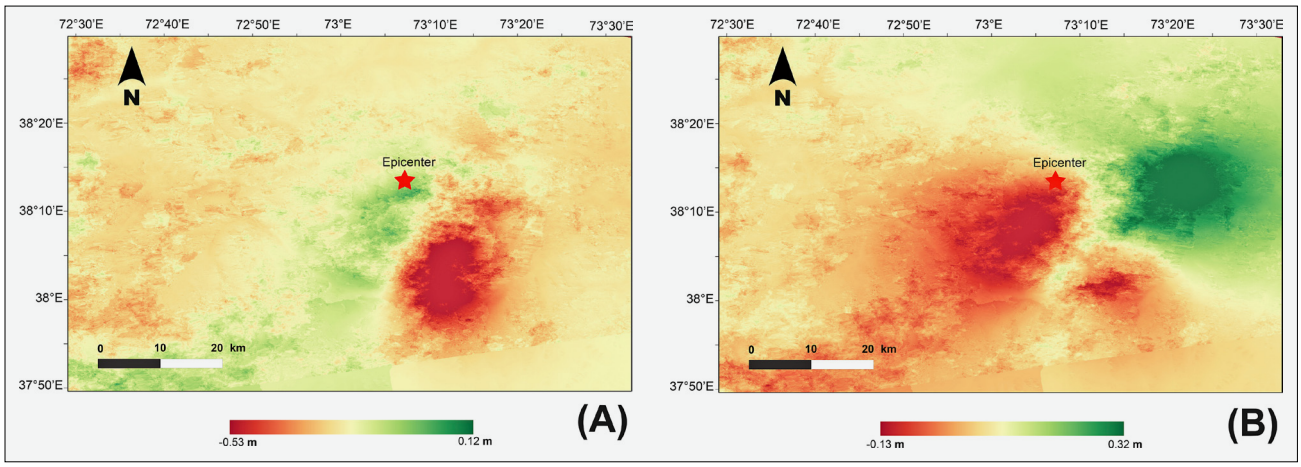

Figure 7. Studying the multi-track InSAR results uncovers (A) east to west horizontal movement and (B) vertical changes in position. The horizontal dimension points to substantial east–west ground activity in the fault sector, whereas the vertical dimension stresses uplift and subsidence dynamics near the epicenter. The data corresponds with strike-slip faulting tied to the seismic phenomenon.

representation of the fault system by incorporating the modelled parameters, offering insight into the earthquake's underlying mechanisms. Lastly, the residual image highlights the discrepancies between the observed and modelled data. It represents the portions of the observed data that the model could not fully explain, pointing to areas where additional complexities or variations remain unaccounted for in the current modelling framework.

The iterative process is critical in producing an effective model. We performed the iteration process eight times, adjusting the iteration count parameter at each step. This iterative approach is vital because it allows the model to be refined through repetition, improving the accuracy of the model's representation of the observed phenomenon. We decided to halt the iterations after reaching 25,000 iterations, as the modelling results at that point were deemed sufficient and aligned with our research objectives. In addition to generating the images, the modelling process yields the best-fit parameters. Our result displayed a calculated fault strike of 128°, with a dip of 67° and a rake of 177°.

3.3. Multi-Track InSAR Result

Figure 7a and **Figure 7b** represent the horizontal (dH) and vertical (dV) displacements, respectively, derived from multi-track InSAR analysis of the 2023 Murghob earthquake in Tajikistan, offering invaluable insight into the surface deformation caused by this significant seismic event. **Figure 7** shows horizontal displacement (dH), with values ranging from -0.53 to 0.12 meters, while Figure 7 depicts vertical displacement (dV) with values between -0.13 and 0.32 meters. Both displacement fields were generated by combining multiple Sentinel-1 radar tracks, allowing for precise separation of horizontal and vertical movement components that would otherwise be hidden in line-of-sight (LOS) data alone. The ability to isolate these movements is crucial for understanding the full extent of tectonic shifts during the earthquake.

4. Discussion

4.1. The essential of Digital Elevation Model (DEM) selection in InSAR processing

Utilizing an external DEM to correct topographic phase is crucial in InSAR processing (**Hanssen, 2002; Furuya, 2011**). A higher spatial resolution DEM can be beneficial in rugged terrain (such as in our study area), since DEM height errors cause residual fringes in the interferogram (**Lazecký et al., 2015**). The high variable topography may be smoothed out in a coarse DEM, which later can cause unwrapping error. However, in relatively flat areas, the difference between using 30 m or 90 m DEM in InSAR processing could be minimal, since the elevation-induced phase is small (**Du et al., 2017**).

4.2. Fault Parameters and Tectonic Complexity of the 2023 Murghob Earthquake

The fault parameters obtained in our study show some differences compared to the results of **Chen et al. (2024); Shi et al. (2023)**, although all studies agree on the dominant right-lateral strike-slip event of the earthquake. In our study, the calculated fault strike was 128°, with a dip of 67° and a rake of 177°, reflecting a high dip, almost vertical fault geometry. On the other hand, **Chen et al. (2024)** observed a strike of 124°, a dip of 86°, and a rake of -147.35°, while **Shi et al. (2023)** reported a strike of 28.08°, a dip of 72.89°, and a rake of -1.85° (see **Table 2**). These variations in fault parameters may arise due to differences in the data sources, modelling techniques, and assumptions used by each study.

Table 2. Parameters comparison with our study

Source	Epicenter		Depth (km)	Fault Plane		
	Longtitude (°)	Latitude (°)		Strike (°)	Dip (°)	Rake (°)
USGS	73.23	38.06	13.5	203	57	-21
gCMT	73.22	38.15	16.9	210	88	1
GFZ	73.29	38.06	10.0	122	73	-156
IPGP	73.208	38.073	8.0	27	73	-20
CENC	73.29	37.98	12.0	313	52	-131
Shi et al., 2023	73.206	38.153	3.67	28.08	72.89	-1.85
Chen et al., 2024	73.2	38.16	16.96	122	86	-147.35
Our study	73.16	38.16	8.51	128	67	177

While our approach integrates 30 m resolution Digital Elevation Models (DEM) and both ascending and descending track InSAR data to achieve detailed spatial resolution of surface deformation, we do not aim to claim methodological superiority over prior studies by institutions such as GFZ (Germany), IPGP (France), USGS, or the Global CMT (gCMT) project. Instead, our study offers a complementary perspective – focusing on the near-surface deformation field and possible complex rupture behaviour. InSAR-based modelling is particularly sensitive to surface displacements and provides a fine-scale view of fault slip distribution, while seismic-based methods such as waveform or moment tensor inversion (e.g. USGS, gCMT) are more effective in characterizing source parameters at depth. Thus, both approaches offer valuable and complementary insight into the rupture process.

In terms of fault geometry, our results align more closely with the models proposed by **Chen et al. (2024)** and GFZ, especially regarding strike and dip values. This alignment may be attributed to the shared reliance on geodetic data and similar inversion methodologies. In contrast, the USGS and gCMT models suggest different orientations and rake angles, possibly generalizing the event as a pure strike-slip rupture. These differences highlight how methodological approaches – InSAR versus seismic inversion – can influence fault parameter interpretations across studies.

The differences in fault geometry and slip characteristics further underline the complexity of the earthquake's seismogenic structure. While prior studies (**Chen et al., 2024; Shi et al., 2023**) focus on the dominant strike-slip component with minor variations in dip and rake angles, our model reveals additional complexity by identifying normal faulting contributions in the northern rupture zone, particularly along the Sarez-Karakul Fault system and the Sarez-Murghab Thrust system. This mixed-slip behaviour, which is less emphasized in other studies, may reflect a more intricate rupture process. Analogous patterns of mixed-mode rupture have been documented in other tectonically complex settings, such as the 2008 Wenchuan (**Lei & Zhao, 2009**) and 2011 Tohoku earthquakes (**Yagi & Fukahata, 2011**), where rupture propagation involved multiple fault systems and mechanisms.

The use of InSAR in our study allows direct measurement of surface deformation at high spatial resolution, making it well suited to identify distributed deformation and possible secondary faulting. However, we recognize the importance of combining this geodetic information with seismic data to better capture the full rupture process from surface to depth.

All three studies – our own, **Chen et al. (2024)**, and **Shi et al. (2023)** – recognize the involvement of multiple fault zones in the rupture. Prior studies. emphasize the Sarez-Karakul and Aksu Murghab fault systems as major contributors **(Chen et al., 2024)**, while **Shi et al. (2023)** focus more heavily on the Sarez-Karakul zone. Our findings are consistent with these, but introduce added complexity by suggesting the involvement of a blind right-lateral strike-slip fault along the eastern segment of the Aksu Murghab Fault system. Additionally, we observe indications of normal and minor left-lateral strike-slip components in the northern rupture area, which were not as clearly detected in other models. These differences further emphasize the tectonic intricacy of the Central Asia collision zone, where oblique convergence between the Indian and Eurasian plates leads to varied faulting styles (**Avouac & Tapponnier, 1993; Singh & Ghosh, 2019; Styron et al., 2011; Tapponnier et al., 2001; Tapponnier, et al., 1981**).

Previous seismic events may also help explain the rupture behaviour of the 2023 earthquake. The 2015 Mw7.2 Murghab earthquake occurred near the epicentral area and involved left-lateral strike-slip and normal faulting in the northern segment (**Sangha et al., 2017**). It likely altered the local stress field, with Coulomb stress transfer potentially promoting failure along the Sarez-Karakul Fault system and other regional structures in 2023 (**Li et al., 2021; Li, et al., 2020; Wang et al., 2017**). Similar triggering effects have been observed in other large strike-slip earthquakes, such as the 1999 Izmit (**Reilinger et al., 2000**) and 1992 Landers events (**Massonnet et al., 1993**).

In conclusion, all major studies agree that the 2023 Tajikistan earthquake was predominantly a right-lateral strike-slip event. However, there are essential differences in fault parameters, geometries, and inferred fault sys-

tem contributions. Our model, which incorporates additional normal faulting and thrust components, adds new dimensions to understanding this rupture. These differences reflect the complexity of the regional tectonics and the complementary nature of diverse modelling techniques. These differences reflect not only the complexity of the regional tectonics but also the complementary nature of diverse modelling techniques. We emphasize that our results are not meant to supersede existing models, but rather to enhance the seismogenic interpretation of this event. We advocate for the continued integration of high-resolution InSAR, seismic data, and tectonic history to develop more complete and accurate assessments of earthquake behaviour in tectonically complex regions like the Pamir and Hindu Kush **(Ischuk et al., 2013; Schurr et al., 2014; Sippl et al., 2013)**.

4.3. Insights into Fault Dynamics and Tectonic Complexity from Multi-Track InSAR Displacements

Vertical displacement can be derived from a single pair of InSAR based on Line of Sight (LoS) and satellite incidence angles (**Cigna & Tapete, 2022**). Nonetheless, the conversion must be carefully taken and assume the movement is only in the vertical direction. Thus, any movement in the horizontal component can have huge inaccuracies (**Fuhrmann & Garthwaite, 2019**). In the region with two SAR tracks (ascending and descending) available, pseudo 3D (2.5 D) can be used (**Fujiwara et al., 2000**).

The vertical displacement (dV) image from multi-track InSAR highlights a predominant upward movement in certain areas, with the positive displacement (green) being more dominant than the negative displacement (red) (see **Figure 7**). This vertical movement suggests the occurrence of uplift, which is consistent with normal faulting or thrust faulting processes that often accompany lateral fault movement in compressional settings. The Sarez-Karakul normal fault and other thrust and strike-slip fault components in the region likely contributed to these vertical shifts.

On the other hand, the horizontal displacement (dH) image reveals significant westward and eastward motions, with red zones indicating negative displacements (westward movement) and green zones showing positive displacements (eastward movement) (see **Figure 7**). This pattern suggests that the earthquake involved lateral fault movements, typical of strike-slip faulting, where two blocks of the Earth's crust move horizontally past each other. The distribution of displacements in these directions aligns with the region's fault system, specifically the Aksu Murghab Fault system, known for its strike-slip characteristics.

The tectonic complexity of the Tajikistan region is further underscored by the various fault systems that interact in the area. Studies such as those by **Chen et al. (2024; Shi et al. (2023)** have highlighted the importance of the Sarez-Karakul Fault system and the Aksu Murghab Fault system as primary contributors to the 2023 earthquake. However, our study adds further detail by suggesting that the rupture also likely involved a blind right-lateral strike-slip fault, primarily driven by the Aksu Murghab Fault system in the east. Additionally, we observe influences of normal faulting and left-lateral strike-slip faulting in the northern part of the region, which were less emphasized in previous studies.

The region's tectonic setting is further complicated by its position within the broader Central Asia collision zone, where the Indian and Eurasian plates interact. Various faulting styles characterize this collision zone, including oblique collision, strike-slip faulting, and thrust faulting. The role of these different fault types in shaping the region's tectonic landscape has been well-documented in numerous studies (**Avouac & Tapponnier, 1993; Singh & Ghosh, 2019**). The interactions between these fault systems contribute to the complex seismic activity observed in Tajikistan and surrounding regions. Understanding the contributions of various fault zones to earthquake rupture is essential for improving seismic hazard assessments and developing more effective disaster mitigation strategies in the region.

Additionally, the analysis of horizontal and vertical displacements through multi-track InSAR provides a detailed understanding of the seismic deformations caused by the 2023 Murghob earthquake. The horizontal displacements reveal significant strike-slip faulting, while the vertical displacements suggest a complex combination of uplift and normal faulting. These findings underscore the importance of further research into the fault systems in Tajikistan to better understand the tectonic forces shaping the region and to improve earthquake preparedness and risk assessment.

5. Conclusions

The 2023 Murghob earthquake in Tajikistan, examined through the integration of multi-track InSAR observations and detailed geodetic modelling, reveals a complex rupture process involving multiple fault systems within a tectonically intricate region. The inversion results confirm that the earthquake was predominantly governed by a right-lateral strike-slip mechanism, characterized by a fault strike of 128°, a dip of 67°, and a rake of 177°. Beyond this dominant slip behaviour, the analysis also identifies significant contributions from normal and thrust faulting, particularly concentrated in the northern rupture segment. These findings suggest that the event exhibited a mixed-mode rupture, reflecting the structural complexity of the Pamir tectonic regime. Compared with previously published models (**Chen et al., 2024; Shi et al., 2023**), the fault parameters derived in this study exhibit notable differences. Such discrepancies are likely attributable to variations in

input data, inversion methodologies, and modelling assumptions. Our approach, which combines 30 m Digital Elevation Models (DEMs) with ascending and descending track InSAR datasets, enables improved spatial resolution of surface deformation and fault slip distribution. This methodological framework enhances the capacity to resolve fine-scale features of the rupture, including distributed deformation and secondary fault activation. While our results are broadly consistent with those of **Chen et al. (2024)** and the GFZ model in terms of strike and dip values, the present study contributes several novel insights. These include the potential involvement of a blind right-lateral strike-slip fault along the eastern segment of the Aksu Murghab Fault system, as well as the identification of minor left-lateral and normal faulting components in the northern rupture area – features that have not been prominently reported in prior seismic-only analyses. Such observations highlight the complex nature of fault interactions in this region and underscore the utility of InSAR in capturing near-surface deformation patterns that are not always discernible through seismic data alone. The findings presented here affirm the value of integrating geodetic and seismic data to comprehensively understand earthquake rupture dynamics, from the surface to seismogenic depths. Rather than replacing existing models, this study provides a complementary interpretation that refines the broader seismotectonic characterization of the 2023 event. Further investigations should be planned to enhance the robustness of these interpretations. These include joint inversions incorporating InSAR and seismic waveform data, field-based validation of surface rupture features, and Coulomb stress transfer modelling to assess fault interaction and potential triggering effects. Additionally, time-series InSAR analyses will be employed to monitor postseismic deformation. These future efforts aim to improve regional seismic hazard assessments and support more effective earthquake preparedness and risk mitigation strategies in the broader Pamir and Hindu Kush regions.

Acknowledgement

The authors are grateful for the insightful feedback from the anonymous reviewers. We also thank the European Space Agency (ESA) for granting free access to Sentinel-1 data.

6. References

Abidin, H. Z., Andreas, H., Meilano, I., Gamal, M., Gumilar, I., & Abdullah, C. I. (2009). Deformasi Koseismik dan Pascaseismik Gempa Yogyakarta 2006 dari Hasil Survei GPS. *Indonesian Journal on Geoscience*, *4*(4). https://doi.org/10.17014/ijog.v4i4.87

Avouac, J.-P., & Tapponnier, P. (1993). *Kinematic Model of Active Deformation in Central Asia* (Vol. 20).

Chen, C., & Zebker, H. (2001). Two-dimensional phase unwrapping with use of statistical models for cost functions in nonlinear optimization. *Journal of the Optical Society of America. A, Optics, Image Science, and Vision*, *18*, 338–351. https://doi.org/10.1364/JOSAA.18.000338

Chen, R., Li, J., Liu, D., Yushan, A., Li, R., & Kong, X. (2024). InSAR coseismic deformation and seismogenic structure of the 2023 MW6.9 Tajikistan earthquake. *Geodesy and Geodynamics*. https://doi.org/10.1016/j.geog.2023.12.004

Cigna, F., & Tapete, D. (2022). Land Subsidence and Aquifer-System Storage Loss in Central Mexico: A Quasi-Continental Investigation With Sentinel-1 InSAR. *Geophysical Research Letters*, *49*(15). https://doi.org/10.1029/2022GL098923

Du, Y., Feng, G., Li, Z., Peng, X., Zhu, J., & Ren, Z. (2017). Effects of external digital elevation model inaccuracy on StaMPS-PS processing: A case study in Shenzhen, China. *Remote Sensing*, *9*(11). https://doi.org/10.3390/rs9111115

Fuhrmann, T., & Garthwaite, M. C. (2019). Resolving three-dimensional surface motion with InSAR: Constraints from multi-geometry data fusion. *Remote Sensing*, *11*(3). https://doi.org/10.3390/rs11030241

Fujiwara, S., Nishimura, T., Murakami, M., Nakagawa, H., Tobita, M., & Rosen, P. A. (2000). 2.5-D surface deformation of M6.1 earthquake near Mt Iwate detected by SAR interferometry. *Geophysical Research Letters*, *27*(14), 2049–2052. https://doi.org/10.1029/1999GL011291

Funning, G. J., & Garcia, A. (2019). A systematic study of earthquake detectability using Sentinel-1 InterferometricWide-Swath data. *Geophysical Journal International*, *216*(1), 332–349. https://doi.org/10.1093/gji/ggy426

Furuya, M. (2011). SAR Interferometry. In H. K. Gupta (Ed.), *Encyclopedia of Solid Earth Geophysics* (pp. 1041–1049). Dordrecht: Springer Netherlands. https://doi.org/10.1007/978-90-481-8702-7_97

Furuya, M., Suzuki, T., Maeda, J., & Heki, K. (2017). Midlatitude sporadic-E episodes viewed by L-band split-spectrum InSAR. *Earth, Planets and Space*, *69*(1). https://doi.org/10.1186/s40623-017-0764-6

Goldstein, R. M., & Werner, C. L. (1998). Radar interferogram filtering for geophysical applications. *Geophysical Research Letters*, *25*(21), 4035–4038. https://doi.org/10.1029/1998GL900033

Hanssen, R. F. (2002). *Radar Interferometry, Data Interpretation and Error Analysis*.

He, L., Feng, G., Xu, W., Wang, Y., Xiong, Z., Gao, H., & Liu, X. (2023). Coseismic Kinematics of the 2023 Kahramanmaras, Turkey Earthquake Sequence From InSAR and Optical Data. *Geophysical Research Letters*, *50*(17). https://doi.org/10.1029/2023GL104693

Heimann, S., Isken, M., Kühn, D., Sudhaus, H., Steinberg, A., Vasyura-Bathke, H., … Dahm, T. (2018). *Grond - A probabilistic earthquake source inversion framework*. https://doi.org/10.5880/GFZ.2.1.2018.003

Heimann, S., Kriegerowski, M., Isken, M. P., Cesca, S., Daout, S., Grigoli, F., … Dahm, T. (2017). *Pyrocko - An open-source seismology toolbox and library*. Retrieved from https://api.semanticscholar.org/CorpusID:217360137

Ischuk, A., Bendick, R., Rybin, A., Molnar, P., Khan, S. F., Kuzikov, S., … Zubovich, A. V. (2013). Kinematics of the pamir and hindu kush regions from gps geodesy. *Journal of Geophysical Research: Solid Earth*, *118*(5), 2408–2416. https://doi.org/10.1002/jgrb.50185

Isken, M. P., Sudhaus, H., Heimann, S., Steinberg, A., Daout, S., & Vasyura-Bathke, H. (2017). *Kite - Software for Rapid Earthquake Source Optimisation from InSAR Surface Displacement*. Retrieved from https://api.semanticscholar.org/CorpusID:217349180

Lazecký, M., Bakon, M., & Hlavácová, I. (2015). Effect of DEM inaccuracy on precision of satellite inSAR results. *Lecture Notes in Geoinformation and Cartography*, *211*, 165–171. Kluwer Academic Publishers. https://doi.org/10.1007/978-3-319-18407-4_14

Lei, J., & Zhao, D. (2009). Structural heterogeneity of the Longmenshan fault zone and the mechanism of the 2008 Wenchuan earthquake (Ms 8.0). *Geochemistry, Geophysics, Geosystems*, *10*(10). https://doi.org/10.1029/2009GC002590

Li, Y., Huang, L., Ding, R., Yang, S., Liu, L., Zhang, S., & Liu, H. (2021). Coulomb stress changes associated with the M7.3 Maduo earthquake and implications for seismic hazards. *Natural Hazards Research*, *1*(2), 95–101. https://doi.org/10.1016/j.nhres.2021.06.003

Li, Y., Shao, Z., Shi, F., & Chen, L. (2020). Stress evolution on active faults in the southwestern Yunnan region, southeastern Tibetan Plateau, and implications for seismic hazard. *Journal of Asian Earth Sciences*, *200*. https://doi.org/10.1016/j.jseaes.2020.104470

Liu, Y., Wu, S., Zhang, B., Xiong, S., & Wang, C. (2024). Accurate Deformation Retrieval of the 2023 Turkey–Syria Earthquakes Using Multi-Track InSAR Data and a Spatio-Temporal Correlation Analysis with the ICA Method. *Remote Sensing*, *16*(17), 3139. https://doi.org/10.3390/rs16173139

Massonnet, D., & Feigl, K. L. (1998). Radar interferometry and its application to changes in the earth's surface. *Reviews of Geophysics*, *36*(4), 441–500. https://doi.org/10.1029/97RG03139

Massonnet, D., Rossi, M., Cesar, C., Adragna, F., Peltzer, G., Feigl, K., & Rabaute, T. (1993). The Displacement Field of The Landers Earthquake Mapped by Radar Interferometry. *Nature*, *364*, 138–142.

R. E. Reilinger, S. Ergintav, R. Burgmann, S. McClusky, O. Lenk, A. Barka, … M. N. Toksoz. (2000). *Coseismic and Poseismic Fault Slip for the 17 August 1999 M=7.5, Izmit, Turkey Earthquake*. https://doi.org/DOI:10.1126/science.289.5484.1519

Sangha, S., Peltzer, G., Zhang, A., Meng, L., Liang, C., Lundgren, P., & Fielding, E. (2017). Fault geometry of 2015, Mw7.2 Murghab, Tajikistan earthquake controls rupture propagation: Insights from InSAR and seismological data. *Earth and Planetary Science Letters*, *462*, 132–141. https://doi.org/10.1016/j.epsl.2017.01.018

Schurr, B., Ratschbacher, L., Sippl, C., Gloaguen, R., Yuan, X., & Mechie, J. (2014). Seismotectonics of the Pamir. *Tectonics*, *33*(8), 1501–1518. https://doi.org/10.1002/2014TC003576

Setiawan, N., & Furuya, M. (2021). Tropospheric dispersive phase anomalies during heavy rain detected by L-band InSAR and their interpretation. *Earth, Planets and Space*, *73*(1). https://doi.org/10.1186/s40623-021-01470-9

Setiawan, Naufal, & Furuya, M. (2024). Heavy Rain Episodes Identified by L-band InSAR and Limitations of Split-Spectrum Method in Indonesia. *Geosfera Indonesia*, *9*(1), 1. https://doi.org/10.19184/geosi.v9i1.38154

Shi, Y., Wang, Y., & Bian, Y. (2023). Coseismic Source Model of the February 2023 Mw 6.8 Tajikistan Earthquake from Sentinel-1A InSAR Observations and Its Associated Earthquake Hazard. *Remote Sensing*, *15*(12). https://doi.org/10.3390/rs15123010

Singh, S., & Ghosh, A. (2019). Surface Motions and Continental Deformation in the Indian Plate and the India-Eurasia Collision Zone. *Journal of Geophysical Research: Solid Earth*, *124*(11), 12141–12170. https://doi.org/10.1029/2018JB017289

Sippl, C., Schurr, B., Yuan, X., Mechie, J., Schneider, F. M., Gadoev, M., … Radjabov, N. (2013). Geometry of the Pamir-Hindu Kush intermediate-depth earthquake zone from local seismic data. *Journal of Geophysical Research: Solid Earth*, *118*(4), 1438–1457. https://doi.org/10.1002/jgrb.50128

Styron, R. H., Taylor, M. H., & Murphy, M. A. (2011). Oblique convergence, arc-parallel extension, and the role of strike-slip faulting in the High Himalaya. *Geosphere*, *7*(2), 582–596. https://doi.org/10.1130/GES00606.1

Tapponnier, P., Zhiqin, X., Roger, F., Meyer, B., Arnaud, N., Wittlinger, G., & Jingsui, Y. (2001, November 23). Oblique stepwise rise and growth of the tibet plateau. *Science*, Vol. 294, pp. 1671–1677. https://doi.org/10.1126/science.105978

Tapponnier, Paul, Mattauer, M., Proust, F., & Cassaigneau, C. (1981). Mesozoic ophiolites, sutures, and large-scale tectonic movements in Afghanistan. In *Earth and Planetary Science Letters* (Vol. 52).

USGS Earthquake Hazard Program. (n.d.). Retrieved from https://earthquake.usgs.gov/earthquakes/eventpage/us6000jqxc/executive

Wang, J., Xu, C., Freymueller, J. T., & Li, Z. (2017). Probing Coulomb stress triggering effects for a Mw > 6.0 earthquake sequence from 1997 to 2014 along the periphery of the Bayan Har block on the Tibetan Plateau. *Tectonophysics*, *694*, 249–267. https://doi.org/10.1016/j.tecto.2016.11.009

Wright, T. J., Parsons, B. E., & Lu, Z. (2004). Toward mapping surface deformation in three dimensions using InSAR. *Geophysical Research Letters*, *31*(1). https://doi.org/10.1029/2003GL018827

Yagi, Y., & Fukahata, Y. (2011). Rupture process of the 2011 Tohoku-oki earthquake and absolute elastic strain release. *Geophysical Research Letters*, *38*(19). https://doi.org/10.1029/2011GL048701

Zhou, Y., He, J., Oimahmadov, I., Gadoev, M., Pan, Z., Wang, W., … Rajabov, N. (2016). Present-day crustal motion around the Pamir Plateau from GPS measurements. *Gondwana Research*, *35*, 144–154. https://doi.org/10.1016/j.gr.2016.03.011

SAŽETAK

Seizmogena analiza potresa magnitude 6,9 u Murghobu 2023. godine, Tadžikistan, temeljena na Multi-Track InSAR tehnici i modeliranju

Ova studija istražuje potres u Murghobu u Tadžikistanu 2023. godine (Mw 6,9) korištenjem modeliranja i Multi-Track InSAR tehnike s ciljem definiranja deformacija površine i dinamike rasjeda. Pyrocko pristup modeliranju rezultirao je stvaranjem opažačkih, modeliranih i rezidualnih slika, od kojih svaka otkriva određene aspekte geometrije rasjeda i karakteristika loma. Naša studija identificirala je dominantni događaj desnoga lateralnog pomaka po pružanju, s izračunanim pravcem pružanja rasjeda od 128–308°, smjerom nagiba 218°, kutom nagiba od 67° i smjerom pomaka krovine prema azimutu 177°. Nadalje, modeliranje je također uputilo na postojanje dijagonalnoga pomaka po rasjedu, uključujući komponente normalnoga rasjedanja duž rasjednoga sustava Sarez-Karakul i navlačnoga sustava Sarez-Murghab. Ta saznanja upućuju na složeniji proces rasjedanja nego što je prethodno naglašavano u drugim modelima. Multi-Track InSAR analiza podržala je ove rezultate mjerenjima visoke rezolucije horizontalnih (dH) i vertikalnih (dV) pomaka. Horizontalni pomaci otkrili su znatne pomake po pružanju (–0,53 do 0,12 metara) duž rasjednoga sustava Aksu Murghab. U međuvremenu vertikalni pomaci uputili su na znatno izdizanje (–0,13 i 0,32 metra), vjerojatno zbog interakcije između normalnih rasjeda i navlaka. Rezultati ističu postojanje složenoga tektonskog okruženja u regiji, na koje utječu višestruki rasjedni sustavi, uključujući rasjede Sarez-Karakul i Aksu Murghab. Rezultati istraživanja naglašavaju važnost integriranja različitih geofizičkih metoda kako bi se bolje razumjeli mehanizmi potresa i poboljšale procjene seizmičke opasnosti u tektonski aktivnim regijama poput Tadžikistana.

Ključne riječi:
InSAR, Multi-Track InSAR, modeliranje potresa, potres u Murghobu 2023. godine

Author's contribution

Rana Jaladara: conceptualization, processing data, writing – original draft and editing, visualization, validation, data curation, and formal analysis. **Naufal Setiawan**: conceptualization, methodology, writing – original draft and editing, validation, investigation, and formal analysis. **Erlan Sumanjaya**: methodology, writing – original draft and editing, validation, investigation, and formal analysis.
All authors have read and agreed to the published version of the manuscript.